Analysis of the Emission Features in Graded-Index Polymer Optical Fiber Amplifiers

Igor Ayesta, Jon Arrue, Felipe Jiménez, María Asunción Illarramendi, and Joseba Zubia

***Abstract*—Organic dye-doped polymer optical fiber amplifiers (POFAs) are suitable for achieving high gains in short distances in the visible region. This paper presents a computational analysis of the optimum pump power and signal wavelength as a function of fiber length, numerical aperture, and radial distribution of dopant, for the case of a graded-index POFA doped with rhodamine B.**

***Index Terms*—Doped fiber amplifiers, dye-density distribution, numerical aperture, polymer optical fiber (POF), rhodamine B (RB).**

I. Introduction

POLY (methyl methacrylate) (PMMA) polymer optical fibers (POFs) have raised a great interest in applications such as local area networks, sensors and, more recently, also in the field of fiber lasers and amplifiers in the visible region, since many choices of organic dopants are available for such fibers. The main advantage of organic dyes is that they exhibit very large absorption and emission cross sections. Their spectral shape and height are determining factors in the spectral gain of the doped fiber [1]–[11]. The maximum gain usually takes place near the peak wavelength of the emission cross section [9], [12]. These characteristics of organic dyes allow the manufacture of compact fiber amplifiers based on such dyes, which are highly compatible with POFs. The aim of such amplifiers is to extend significantly the length of the POF link in which they are incorporated, which can be of hundreds of meters [2]. The organic dye rhodamine B (RB), for example, allows amplification in the visible region. Its large emission and absorption cross sections (10 000 times larger than those of Er^{3+} in glass) serve to obtain high gains in particularly short fiber lengths [4]. It can be easily dispersed in PMMA POFs to obtain graded-index (GI) or step-index (SI) POF amplifiers (POFAs). The main advantage of passive GI POFs is that their bandwidth is typically two orders of magnitude larger than that of SI POFs [10]. On the other hand, the dye must have high photochemical stability, to be able to withstand multiple excitation cycles with a pulsed pump laser [10]. In this respect, the photostability achieved with RB-doped POFs is greater than that accomplished with most of dyes. It is also greater with optical fibers than with any other host [4], [5]. There are other organic dopants, such as conjugated polymers, that have faster transitions than RB and which can be employed for amplification in other wavelengths and also for switching [13], [14]. However, if high-energy photons are used (as in the proximity of the ultraviolet region), photobleaching can occur [15], which limits the maximum energy of the pump pulses. Therefore, efforts are being made to produce new conjugated polymers and oligomers whose working range is shifted toward the visible region, in order to avoid photobleaching effects at high pump energies [16]. The dye RB is suitable to obtain higher gains than with other dopants and to work in the wavelengths of low attenuation in POFs (from the final part of the green color to the beginning of the red). This paper focuses on some parameters of GI POFAs that have not been analyzed in detail yet.

Specifically, we carry out a computational analysis of the optimum pump power and signal wavelength as a function of fiber length, numerical aperture, and radial distribution of the active dopant in GI POFs. For this purpose, we have worked with a mathematical model that serves to analyze both the temporal and spectral characteristics of light in dye-doped POFs for any traveled distance z. The model has been adapted to take into account the nonuniform dopant and light power distributions, by means of an overlapping factor γ. It has also been adapted to study the average influence of the nonuniform fiber numerical aperture NA, by means of an average parameter called β. As for γ, it is only necessary when we deal with GI POFs (otherwise its value is 1). It has been quantified by means of an integral that takes into account the normalized product between the dye density distribution and the power density distribution, which will be defined later.

This paper is organized as follows. The governing equations adapted from our previous model for SI POFAs [12] are presented in Section II. The results obtained for GI POFAs are shown and discussed in Section III. The conclusions are summarized in Section IV.

Manuscript received March 29, 2011; revised June 04, 2011; accepted July 08, 2011. Date of publication July 14, 2011; date of current version August 19, 2011. This work was supported by the Ministerio de Ciencia e Innovació n under projects TEC2009-14718-C03-01 and COBOR, by the Gobierno Vasco/Eusko Jaurlaritza under projects GIC07/156-IT-343-07, AIRHEM, S-PR10UN04, and S-PE10CA01, and by the Diputación Foral de Bizkaia/Bizkaiko Foru Aldundia under project 06-12-TK-2010-0022. The research leading to these results has also received funding from the European Commission's Seventh Framework Programme under Grant agreement 212912 (AISHA II). The work of I. Ayesta was supported in part by a research fellowship from Vicerrectorado de Euskara y Plurilingüismo, Universidad del País Vasco/Euskal Herriko Unibertsitatea (UPV/EHU), while working on the Ph.D. degree.

I. Ayesta, J. Arrue, and J. Zubia are with the Department of Electronics and Telecommunications, E.T.S.I. of Bilbao, University of the Basque Country (UPV/EHU), Bilbao 48013, Spain (e-mail: igor.ayesta@ehu.es; jon.arrue@ehu.es; joseba.zubia@ehu.es).

F. Jiménez is with the Department of Applied Mathematics, E.T.S.I. of Bilbao, University of the Basque Country (UPV/EHU), Bilbao 48013, Spain (e-mail: felipe.jimenez@ehu.es).

M. A. Illarramendi is with the Department of Applied Physics I, E.T.S.I. of Bilbao, University of the Basque Country (UPV/EHU), Bilbao 48013, Spain (e-mail: ma.illarramendi@ehu.es).

Digital Object Identifier 10.1109/JLT.2011.2162102

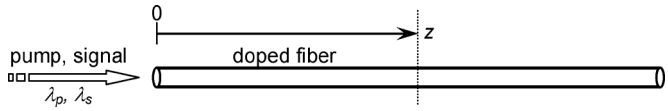

Fig. 1. Longitudinal pumping of light at a wavelength λ_p in an active POF, with signal at λ_s.

II. Governing Equations for GI POFAs

In order to analyze GI POFAs, we have adapted the set of partial differential equations, initial conditions, and boundary conditions for SI POFAs described in [12]. Specifically, we take into account the overlap between the dye-concentration distribution and the light-density distribution in GI POFs. We have also modified the equations to take into account the fiber numerical aperture (its average value, since it depends on the radial distance r in the case of a GI POF). We obtain the light power for each time t, wavelength λ, and distance z (see Fig. 1).

The total dopant molecular concentration per unit volume N is time independent. Assuming that the transitions of organic dyes are described with two main electronic energy levels, N is the sum of the excited (N_2) and the nonexcited (N_1) molecular concentrations, i.e., $N = N_1 + N_2$. The equations reported in [12] could be used without changes if N were distributed uniformly, irrespective of the radial distance r from the center of the fiber symmetry axis. However, the manufacturing techniques used to introduce the active dopant into a GI POF yield higher concentrations near the fiber symmetry axis, where GI fibers propagate more light. This greater light power density at points in which the dopant concentration is higher happens because light rays tend to constantly bend toward the fiber symmetry axis, where the refractive index is maximum. Therefore, in that area both the dopant molecular concentration and the photon concentration are higher than average, so the probabilities that they interact are higher than average too. To take this into account, a correction factor $\gamma > 1$ must be introduced into every term of the governing equations where there is a product of dopant concentration and light power [1], [2]. By using γ, the governing equations to obtain the fraction of power at each wavelength λ_k are as follows:

$$\frac{\partial P_p}{\partial z} = -\sigma^a(\lambda_p) N_1 P_p \gamma - \frac{1}{v_z}\frac{\partial P_p}{\partial t} \tag{1}$$

$$\begin{aligned}\frac{\partial N_2}{\partial t} = {} & \frac{-N_2}{\tau} - \left(\frac{\sigma^e(\lambda_k)}{h(c/\lambda_k)A_c}\right) N_2 P_s \gamma \\ & + \left(\frac{\sigma^a(\lambda_p)}{h(c/\lambda_p)A_c}\right) N_1 P_p \gamma \\ & + \left(\frac{\sigma^a(\lambda_k)}{h(c/\lambda_k)A_c}\right) N_1 P_s \gamma\end{aligned} \tag{2}$$

$$\begin{aligned}\frac{\partial P_s}{\partial z} = {} & \sigma^e(\lambda_k) N_2 P_s \gamma - \sigma^a(\lambda_k) N_1 P_s \gamma - \frac{1}{v_z}\frac{\partial P_s}{\partial t} \\ & + \frac{N_2}{\tau}\frac{hc}{\lambda_k}\sigma^e_{sp}(\lambda_k)\beta A_c\end{aligned} \tag{3}$$

Here, P_p and P_s are the pump and signal powers. σ^a and σ^e are the absorption and emission cross sections. Their values for the case of RB have been taken from [2]. The parameters A_c and h are the cross section of the fiber core and Planck's constant, respectively. The propagation velocity along z is represented as v_z, and τ is the fluorescence lifetime of the dye, which is 2.85 ns in the case of RB [17].

There are two main differences in the equations with respect to those employed in [12]: on one hand, the aforementioned overlapping factor γ is used in any term in which either P_s or P_p appears multiplied by N_1 or N_2, and on the other hand, an average value of β should be calculated, so as to take into account that the numerical aperture NA varies with r in GI fibers.

According to [1], the overlapping factor can be defined as

$$\gamma = \int_0^{a_0} \theta(r)\psi(r) 2\pi r dr \tag{4}$$

where $\theta(r)$ and $\psi(r)$ are the normalized dye density distribution and the power density distribution, respectively, and a_0 is the core radius. The physical meaning of $\psi(r)$ and $\theta(r)$ can be interpreted from the following relationships: we can define $I(t,z,r) = P(t,z)\psi(r)$, where $P(t,z)$ (in watts) is the total power in the cross section at a given t and z, and $\psi(r)$ is a factor to obtain the light density I (in W/m^2) at r and those t and z [2]. Similarly, we can define the molecular density per unit volume at each distance r as $n(t,z,r) = N(t,z)\theta(r)$, where $N(t,z)$ is the average molecular density in a differential slice of fiber at t and z, and $\theta(r)$ (nondimensional) accounts for the radial dependence. The way to normalize both distributions is as follows. As stated earlier, if both $\theta(r)$ and $\psi(r)$ were constant (θ_0 and ψ_0, respectively), then γ would be 1, so

$$\int_0^{a_0} \theta_0\psi_0 2\pi r dr = 1 \quad \Rightarrow \quad \theta_0\psi_0 = \frac{1}{\pi a_0^2}. \tag{5}$$

Since θ_0 is the average dopant concentration

$$\begin{aligned}\int_0^{a_0} \theta(r) 2\pi r dr &= \int_0^{a_0} \theta_0 2\pi r dr \\ &\Rightarrow \int_0^{a_0} \theta(r) r dr = \theta_0 \frac{a_0^2}{2}.\end{aligned} \tag{6}$$

And similarly for the light power

$$\int_0^{a_0} \psi(r) r dr = \psi_0 \frac{a_0^2}{2}. \tag{7}$$

Usually, graphs of nonnormalized dopant and light power distributions are reported [2], [5], [18]. Let us call them $\theta_{nn}(r)$ and $\psi_{nn}(r)$, respectively. Their normalized counterparts are proportional to them

$$\theta(r) = k_1\theta_{nn}(r), \quad \psi(r) = k_2\psi_{nn}(r). \tag{8}$$

From (6) and (7), the values of k_1 and k_2 in (8) are

$$\begin{aligned}k_1 &= \theta_0 \frac{a_0^2}{2} \Big/ \int_0^{a_0} \theta_{nn}(r) r dr \\ k_2 &= \psi_0 \frac{a_0^2}{2} \Big/ \int_0^{a_0} \psi_{nn}(r) r dr.\end{aligned} \tag{9}$$

Finally, from (4) and using (5), (8), and (9)

$$\gamma = \frac{a_0^2}{2} \frac{\int_0^{a_0} \theta_{nn}(r)\psi_{nn}(r) r dr}{\int_0^{a_0} \theta_{nn}(r) r dr \int_0^{a_0} \psi_{nn}(r) r dr}. \tag{10}$$

The data needed to evaluate γ numerically using (10) are available from Fig. 5 reported in [2]. The result that we have obtained for the integral using such figure is $\gamma = 1.43$. Although γ could take any value from 0 to ∞, realistic values are not very different from 1.4. For example, $\gamma = 1.53$ can be obtained from [5] and $\gamma = 1.36$ from [18]. Our results, except for graphs comparing different values of γ, correspond to $\gamma = 1.43$ (obtained from [2]). The graphs for several values of γ will show that the greater the γ is, the higher the gain of the GI POFA tends to be, which is an advantage of GI POFAs over SI POFAs, for which $\gamma = 1$.

In optical amplifiers, signal gain at a wavelength λ is defined as

$$G(\lambda)\ (\mathrm{dB}) = 10\log_{10}\left(\frac{P_{\mathrm{out}}(\lambda) - P_{\mathrm{ASE}}(\lambda)}{P_{s,\mathrm{in}}(\lambda)}\right). \tag{11}$$

In this formula, $P_{s,\mathrm{in}}(\lambda)$ is the power of the input signal centered at wavelength λ. The numerator is the difference between the power of the amplified signal at the output of the POFA and the power of the background of amplified spontaneous emission (ASE) over the same range of wavelengths where the amplified signal appears. In other words, the numerator is the output power attributable to the amplified signal only. Note that a simpler definition of gain in which P_{ASE} is not subtracted ("total gain") would tend to coincide with this one when the signal power is high.

We will also see that the influence of the fiber numerical aperture on the signal gain of a POFA is smaller than that of γ. We want to remark that the influence of the numerical aperture is much greater in a POF laser than in a POFA, due to the fact that the ASE is useful in a laser, but not in a signal amplifier.

The influence of the numerical aperture is introduced in the equations through the parameter β. The direction of spontaneous photons is isotropically random, so only a fraction β of them can contribute to signal amplification in guided directions. The value of β is equal to the fraction of spontaneous emissions lying in guided directions in the fiber, assuming that all of them will eventually contribute to stimulated emissions. For a fiber whose maximum core refractive index is n_1 and whose cladding refractive index is n_2, we can estimate the value of β at the fiber axis β_0 by means of the following quotient:

$$\beta_0 = \frac{\int_0^{\theta_c} I_0 2\pi \sin\theta d\theta}{\int_0^{\pi} I_0 2\pi \sin\theta d\theta} = \frac{1-\cos\theta_c}{2} = \frac{n_1 - n_2}{2n_1} \simeq \frac{\mathrm{NA}_0^2}{4n_1^2} \tag{12}$$

in which I_0 is the light intensity (in W/sr) emitted spontaneously by an atom and θ_c is the complementary critical angle [19]. Therefore, β_0 is proportional to the relative difference of refractive indexes, which is approximately proportional to the square of the maximum numerical aperture (NA_0) of the GI fiber (at $r = 0$). If the dye concentration were constant, the fraction of guided directions as a function of r, which we have called $\beta_r(r)$, would be

$$\beta_r(r) \simeq \beta_0\left[1 - \left(\frac{r}{a_0}\right)^2\right] \tag{13}$$

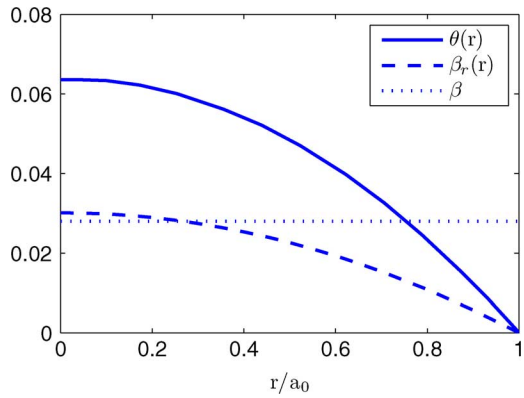

Fig. 2. β (average value) obtained from (14) for a typical GI POF, in which $\theta(r)$ and $\beta_r(r)$ decrease with r as shown in the solid and dashed curves.

i.e., it would have the same shape as NA $(r)^2$. However, we can generalize the previous expression to take into account that the distribution of dye concentration is a function of r, so $\beta_r(r)$ should be weighted proportionally both to r (since the differential area is $\mathrm{dA} = 2\pi r dr$) and $\theta(r)$. Specifically, the average value of β is obtained as follows:

$$\beta = \frac{\int_0^{a_0} \beta_r(r)\theta(r) 2\pi r dr}{\int_0^{a_0} \theta(r) 2\pi r dr}. \tag{14}$$

We will maintain $n_1 = 1.492$ in all cases (the same core) and we will consider the influence of the refractive index of the cladding. For the typical value $n_2 = 1.402$, we obtain that β is 0.028, so this will be the average value employed for most of our simulations. Fig. 2 illustrates the corresponding values of $\beta_r(r)$ and of the distribution $\theta(r)$ of dopant concentration, from which (14) yields the aforementioned β (dotted line). On the one hand, we can note that $\beta_r(r)$ decreases with r, which implies smaller total spontaneous emission than in the case of SI POFs with the same NA_0, and therefore, it implies greater signal gains in GI POFAs than in SI ones, as will be shown. On the other hand, $\theta(r)$ is maximum when $r = 0$, where the light density in a GI fiber is also maximum, so $\gamma > 1$. This is an advantage over SI fibers, as will be shown in this paper.

The minimum possible β (average value) is 0, which would happen if $n_1 = n_2$, although this is only a theoretical limit, since it would imply a flat refractive-index profile. The maximum one is approximately 0.15, which happens when $n_2 = 1$, i.e., in an uncladded POF.

Regarding the initial conditions needed to solve (1), (2) and (3), we consider that P_p, P_s, and N_2 are 0 at $t = 0$ for every z. Besides, at the boundary $z = 0$, both the pump and the signal powers are Gaussian pulses in time. Both of them reach their maximum values at the same time. We can employ the numerical scheme that we described in [12], because the equations are basically the same, except for the average value of β and for $\gamma \neq 1$.

III. Computational Results and Discussion

First, by using our computational model, let us analyze to what extent variations in the numerical aperture of the fiber (i.e., in β) affect the threshold power and the gain in GI POFs. The threshold energy refers to the lowest energy of the pump pulse

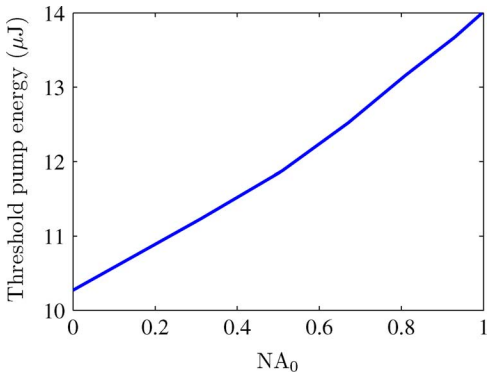

Fig. 3. Threshold pump energy as a function of the numerical aperture at the axis of the fiber described in the text.

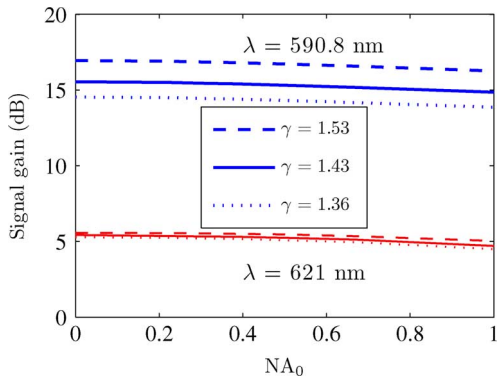

Fig. 4. Signal gain as a function of the numerical aperture at the axis of the fiber, with the parameters described at the beginning of the section. The pump energy is 32.1 μJ (corresponding to a peak power of 5 kW). Two signal wavelengths have been considered.

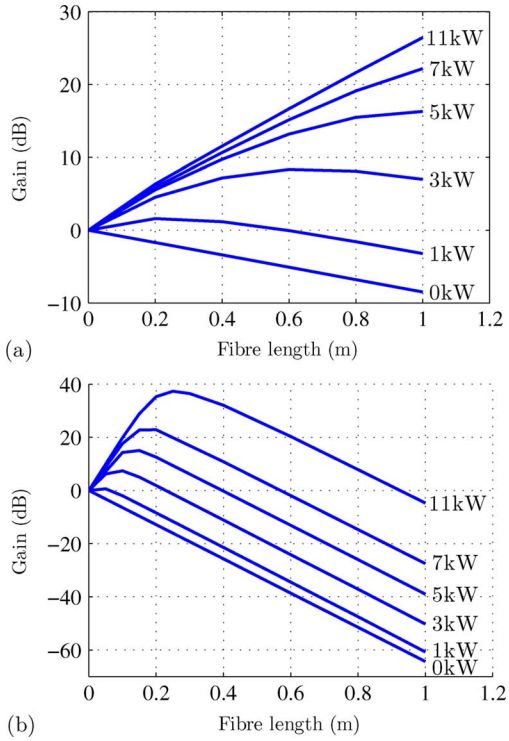

Fig. 5. Signal gain as a function of length for fibers with dye densities of (a) 0.13 ppm and (b) 1 ppm. The rest of the parameters are as described at the beginning of the section.

necessary to obtain amplification of the signal pulse. In order for the results to correspond to a realistic situation, we have used the same parameters as those reported for a GI POFA in [2] and [9], namely the following ones: an RB-doped GI POF of 1 m whose concentration of dopant is 0.13 ppm and whose core diameter is 500 μm; an input signal of 1 W centered at 591 nm whose temporal width is full-width at half-maximum (FWHM) $= 3.5$ ns; and a pump wavelength of 532 nm whose temporal width is FWHM $= 6$ ns and whose peak power will be varied to obtain the threshold. For a Gaussian temporal shape, the total energy of the pump pulse E_p can be related to its peak power $P_{p,\max}$ through the equation $E_p = P_{p,\max}\sqrt{2\pi}\mathrm{FWHM}/2.35$. Fig. 3 shows E_p as a function of the maximum numerical aperture NA_0 of the POF using the aforementioned parameters and the core refractive index $n_1 = 1.492$. We can see that there are great variations in the threshold energy if NA_0 varies. Specifically, it increases significantly when NA_0 increases from 0 to its maximum possible value 1. This is due to the detrimental effect of the spontaneous emission on the signal gain, because it is a differential gain over the ASE power, which increases when NA_0 increases. The dependence is fairly linear, as can be seen.

The signal gain is also slightly dependent on NA_0, as shown in Fig. 4 for three different values of γ and two different signal wavelengths.

We can see (see Fig. 4) that there are slight decreases in gain in all three cases when NA_0 increases from a very small value to 1. The differences are smaller for a wavelength of lower gain (621 nm). As expected, higher gains are achieved if γ grows. For any value of NA_0, there can be differences in gain of about 2 dB when γ varies from one limit to the other of the range obtained from the three aforementioned experimental results [2], [5], [18]. Although γ has a noticeable influence on the signal gain, the three curves have similar slopes, i.e., the influence of γ on the gain does not change with the numerical aperture.

In Figs. 3 and 4, the fiber length was 1 m, but we have also calculated the optimum lengths for several pump powers and dye concentrations. These can be obtained from the maxima in Fig. 5(a) and (b), which correspond to concentrations of 0.13 and 1 ppm, respectively.

As can be seen (see Fig. 5), increasing the dye density of the optical fiber serves to obtain higher gains in shorter distances, and the optimum length decreases as well. In fiber lengths of up to 1 m, maximum gains of about 27 dB can be obtained with dye concentrations of 0.13 ppm, whereas gains of up to 40 dB are obtainable with dye concentrations of 1 ppm. In the following, the concentration of RB will be 0.13 ppm in all the figures.

In Fig. 6, we have plotted together such experimental results and our computational results for the sake of comparison. The figure shows that the obtained gains agree satisfactorily with the experimental ones reported in [2]. The measurements in [2] were carried out for 1 m of PMMA GI POF doped with 0.13 ppm of RB as well. We can note that the gain saturates for high pump powers, which is a well-known effect [20]. The same results as

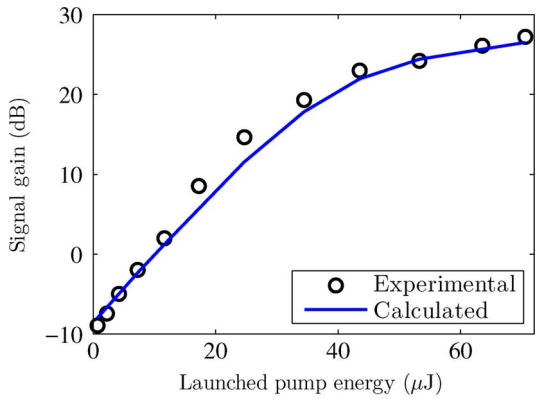

Fig. 6. Comparison between experimental results from [2] (dots) and our computational results (solid line) for the signal gain at $\lambda = 591$ nm for $\gamma = 1.43$ as a function of launched pump energy for a 1 m fiber whose parameters are described at the beginning of the section. $\mathrm{NA}_0 = 0.51$.

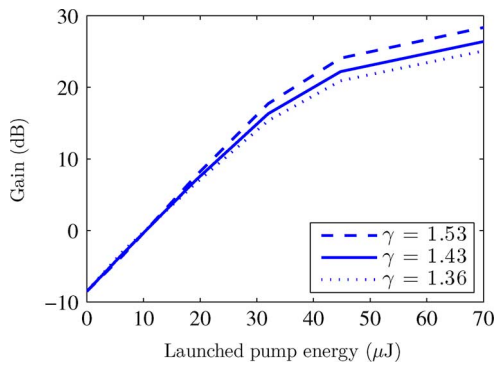

Fig. 7. Variations in signal gain as a function of pump energy for three different values of γ obtained from experimental data. The rest of the parameters are the ones described at the beginning of the section. $\lambda = 591$ nm and $\mathrm{NA}_0 = 0.51$.

in Fig. 6 are obtained for different widths of the pump pulse as long as the pump energy remains constant.

In Fig. 7, we have repeated the same calculations for other values of γ, so as to see how much the gain changes. For a greater generality, the horizontal axis has been expressed in energy units, corresponding to the same interval of peak powers as in Figs. 5 and 6 (for the pulsewidth considered). We can see that the changes in gain with γ are larger when the pump energy increases. With 70 μJ, the gain changes by about 3 dB when γ increases from 1.36 to 1.53, i.e., from the value of γ corresponding to [18] to that corresponding to [5]. Thus, we can see that reasonable changes in γ produce significant changes in gain (more than 1 dB), but this is so only when the pump energy is higher than 20 μJ approximately, as shown in Fig. 7 (with the same parameters as in Fig. 6, except for γ).

So far, the signal wavelength has been 591 nm in all figures. This value is close to that yielding the maximum gain, which depends on the fiber length, as shown in Fig. 8(a) and (b) for a pump energy of 32.1 μJ. For lengths longer than 1 m, an increase in the fiber length produces an increase in the relative effect of the fiber attenuation, especially for shorter wavelengths [see Fig. 8(b)]. As a consequence, when fiber length is increased

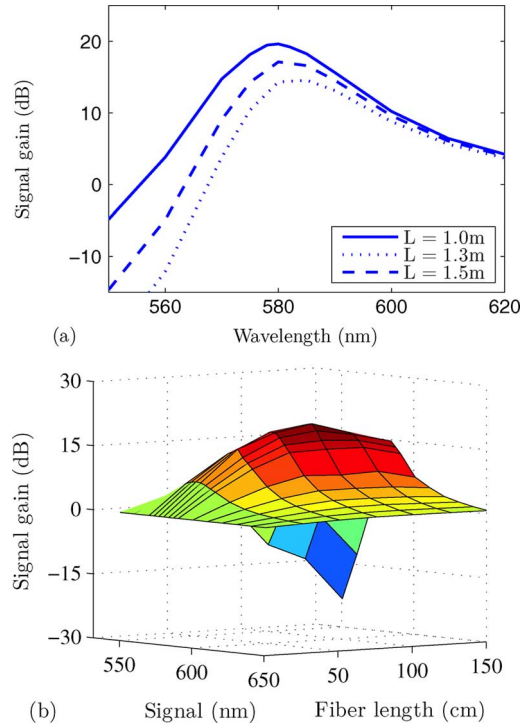

Fig. 8. (a) Signal gain as a function of launched signal wavelength for different fiber lengths. The pump energy is 32.1 μJ, and the fiber parameters are the same as in previous figures, with $\gamma = 1.43$. (b) 3-D figure showing the influence of both the launched signal wavelength (in nanometer) and of the active fiber length (in meter) on the signal gain.

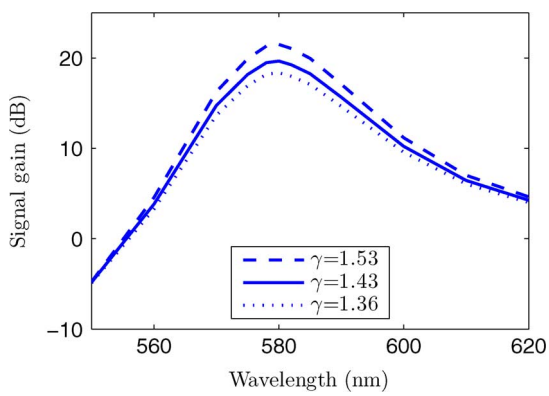

Fig. 9. Signal gain as a function of the launched signal wavelength λ_s (in nanometer) for three different overlapping factors γ that were obtained from experimental data. The fiber length is 1 m, and the other fiber parameters are as in Fig. 8.

from 1 to 1.5 m, the spectrum wavelength is shifted toward longer wavelengths [12].

In Fig. 9, the spectral gain is shown for three different overlapping factors γ that were obtained from experimental data [2], [5], [18]. The corresponding gains differ in about 3 dB in the proximity of the launched signal wavelength yielding maximum gain (581 nm). As can be seen, the signal wavelength is much more influential than γ, and the wavelength of 591 nm used in the experiments is not the most amplified one.

In Fig. 10, we can see that the total gain decreases when the signal energy becomes large, as expected [21], [22]. As for the signal gain, it does not vary so much in the range of input signal

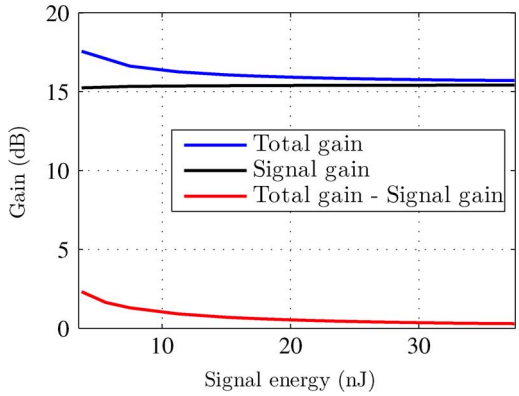

Fig. 10. Total gain (uppermost line) and signal gain (just below it) as a function of signal power for $\lambda = 591$ nm. The other fiber parameters are the same as in Fig. 9 with $\gamma = 1.43$. $\mathrm{NA}_0 = 0.51$. The difference with the total gain is the line at the bottom.

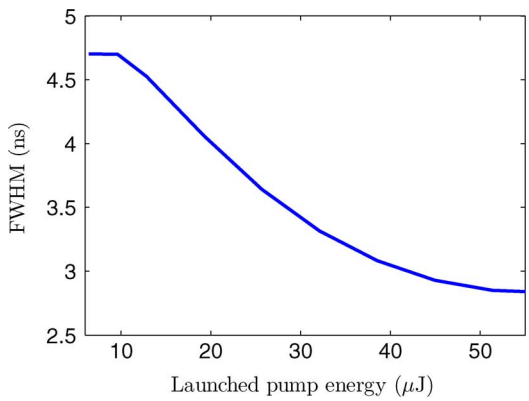

Fig. 11. Output temporal full width at half maximum as a function of pump energy. $\gamma = 1.43$. The other parameters are the ones described at the beginning of the section. $\mathrm{NA}_0 = 0.51$.

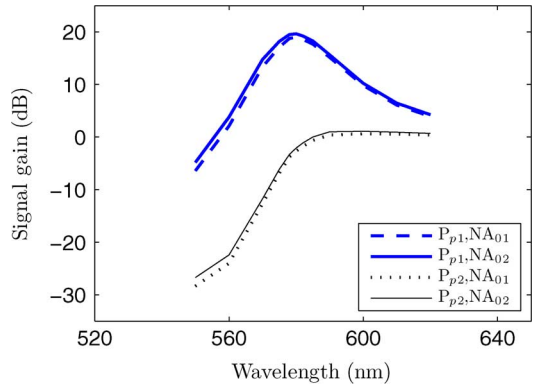

Fig. 12. Signal gain as a function of signal wavelength for two different pump powers ($P_{p1} = 5$ kW, $P_{p2} = 2$ kW) and two different maximum numerical apertures ($\mathrm{NA}_{01} = 1$, $\mathrm{NA}_{02} = 0.51$). $\gamma = 1.43$. The other parameters are the ones described at the beginning of the section.

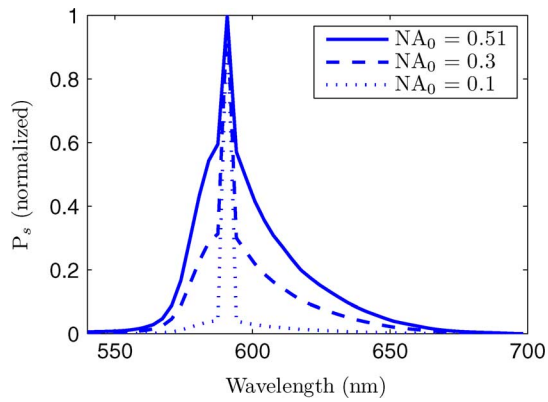

Fig. 13. Normalized output spectrum for three different values of the maximum numerical aperture NA_0. The pump power is 2 kW and $\gamma = 1.43$. The input signal wavelength is 591 nm, and the other parameters are the ones at the beginning of the section.

energies considered, and it tends to have the same value as the total gain when the signal energy is high. The difference between both gains is shown at the bottom of the figure.

Regarding the evolution of the temporal width of the amplified pulse (see Fig. 11), it can be observed that there is a clear narrowing of the signal pulse along 1 m of fiber when the launched pump energy is increased from 10 to 50 μJ (or, more precisely, a smaller broadening from the beginning, where the launched signal pulse was of 3.5 ns). This behavior was also obtained theoretically for SI fibers in [12], and it has been observed experimentally [10].

The evolution of the gain when the fiber is pumped with 2 kW and with 5 kW as a function of the signal wavelength for two different values of the maximum numerical aperture NA_0 is shown in Fig. 12. We can notice that the differences in gain due to increases in NA_0 are almost insignificant in comparison to those caused by changes in the pump power.

Fig. 13 shows the normalized spectrum of the output power as a function of wavelength for three different values of the maximum numerical aperture NA_0 and a signal wavelength of 591 nm. When NA_0 is small, there is only a small fraction of spontaneous emissions that can be guided, so amplification takes place mostly at the wavelength of the input signal, i.e., the output spectrum is very narrow. When NA_0 is greater, the spectrum of P_s broadens.

IV. Conclusion

In this study, we have computationally analyzed the spectral and temporal features of light emission in GI POFAs doped with RB. For this purpose, we have employed *ad hoc* numerical algorithms. The effect of the overlap between the dye-density and power-density radial distributions has been taken into account. Specifically, by introducing an overlapping factor, we have calculated the enhancement of the gain due to the fact that the light power and the dye density are higher than average near the fiber symmetry axis. We have also considered the average effect of the fraction of spontaneous emissions that are guided, by taking into account the nonuniform numerical aperture. Solving the adapted equations, we have analyzed the evolution of the amplification as a function of the maximum numerical aperture of the fiber and the overlapping factor. Depending on the application and on the type of passive POF chosen for the rest of the optical link, GI POFAs or SI POFAs can be employed. The main advantage of GI ones is the better overlapping factor γ, which yields slightly higher gains. The lower average numerical aperture of GI fibers is also beneficial for the signal gain,

although this parameter is less influential than γ. Other parameters studied are the slope efficiency, spectral shifts, optimum signal wavelengths, etc. Our computational results agree satisfactorily with reported experimental data. These analyses can be very useful to develop tunable POF-based optical amplifiers.

REFERENCES

[1] M. Karimi, N. Granpayeh, and M. K. M. Farshi, "Analysis and design of a dye-doped polymer optical fiber amplifier," *Appl. Phys. B (Lasers Opt.)* vol. B78, no. 3–4, pp. 387–396, Feb. 2004.

[2] A. Tagaya, S. Teramoto, T. Yamamoto, K. Fujii, E. Nihei, Y. Koike, and K. Sasaki, "Theoretical and experimental investigation of rhodamine B-doped polymer optical fiber amplifiers," *IEEE J. Quantum Electron.* vol. 31, no. 12, pp. 2215–2220, Dec. 1995.

[3] H. Liang, Z. Zheng, Z. Li, J. Xu, B. Chen, H. Zhao, Q. Zhang, and H. Ming, "Fabrication and amplification of rhodamine B-doped step-index polymer optical fiber," *J. Appl. Polym. Sci.*, vol. 93, pp. 681–685, 2004.

[4] T. Kobayashi, K. Kuriki, N. Imai, T. Tamura, K. Sasaki, Y. Koike, and Y. Okamoto, "High-power polymer optical fiber lasers and amplifiers," in *Proc. Int. Soc. Opt. Eng.*, 1999, vol. 3623, pp. 206–214.

[5] K. Kuriki, T. Kobayashi, N. Imai, T. Tamura, Y. Koike, and Y. Okamoto, "Organic dye-doped polymer optical fiber laser," *Polym. Adv. Technol.*, vol. 11, pp. 612–616, 2000.

[6] M. Rajesh, M. Sheeba, K. Geetha, C. P. G. Vallaban, P. Radhakrishnan, and V. P. N. Nampoori, "Fabrication and characterization of dye-doped polymer optical fiber as a light amplifier," *Appl. Opt.*, vol. 46, pp. 106–112, 2007.

[7] S. Y. Lam and M. J. Damzen, "Characterisation of solid-state dyes and their use as tunable laser amplifiers," *Appl. Phys. B (Lasers Opt.)* vol. B77, no. 6–7, pp. 577–584, Nov. 2003.

[8] A. Tagaya, Y. Koike, T. Kinoshita, E. Nihei, T. Yamamoto, and K. Sasaki, "Polymer optical fiber amplifier," *Appl. Phys. Lett.*, vol. 63, pp. 883–884, 1993.

[9] A. Tagaya, T. Kobayashi, S. Nakatsuka, E. Nihei, K. Sasaki, and Y. Koike, "High gain and high power organic dye-doped polymer optical fiber amplifiers: Absorption and emission cross sections and gain characteristics," *Jpn. J. Appl. Phys.*, vol. 36, pp. 2705–2708, 1997.

[10] A. Tagaya, Y. Koike, E. Nihei, S. Teramoto, K. Fujii, T. Yamamoto, and K. Sasaki, "Basic performance of an organic dye-doped polymer optical fiber amplifier," *Appl. Opt.*, vol. 34, pp. 988–992, 1995.

[11] A. Tagaya, S. Teramoto, E. Nihei, K. Sasaki, and Y. Koike, "High-power and high-gain organic dye-doped polymer optical fiber amplifiers: Novel techniques for preparation and spectral investigation," *Appl. Opt.*, vol. 36, pp. 572–578, 1997.

[12] J. Arrue, F. Jimenez, M. A. Illarramendi, J. Zubia, I. Ayesta, I. Bikandi, and A. Berganza, "Computational analysis of the power spectral shifts and widths along dye-doped polymer optical fibers," *IEEE Photon. J.* vol. 2, no. 3, pp. 521–531, Jun. 2010.

[13] R. Xia, G. Heliotis, Y. Hou, and D. D. C. Bradley, "Fluorene-based conjugated polymer optical gain media," *Organ. Electron.*, vol. 4, pp. 165–177, 2003.

[14] A. Charas, A. L. Mendonça, J. Clark, J. Cabanillas-Gonzalez, L. Bazzana, A. Nocivelli, G. Lanzani, and J. Morgado, "Gain and ultrafast optical switching in PMMA optical fibers and films doped with luminescent conjugated polymers and oligomers," *Front. Optoelectron. China*, vol. 3, pp. 45–53, 2010.

[15] G. D. Peng, Z. Xiong, and P. L. Chu, "Fluorescence decay and recovery in organic dye-doped polymer optical fibers," *J. Lightw. Technol.*, vol. 16, no. 12, pp. 2365–2372, Dec. 2002.

[16] U. Scherf, S. Riechel, U. Lemmer, and R. Mahrt, "Conjugated polymers: Lasing and stimulated emission," *Curr. Opin. Solid State Mater. Sci.*, vol. 5, pp. 143–154, 2001.

[17] D. F. Eaton, "Reference materials for fluorescence measurement," *Pure Appl. Chem.*, vol. 60, pp. 1107–1114, 1988.

[18] K. Sasaki and Y. Koike, "Polymer Optical Fibre Amplifier," U.S. Patent 5 450 232, Sep. 12, 1995.

[19] J. Zubia and J. Arrue, "Plastic optical fibers: An introduction to their technological processes and applications," *Opt. Fiber Technol.: Mater., Devices Syst.* vol. 7, pp. 101–140, Apr. 2001.

[20] M. Kailasnath, T. S. Sreejaya, R. Kumar, C. P. G. Vallabhan, V. P. N. Nampoori, and P. Radhakrishnan, "Fluorescence characterization and gain studies on a dye-doped graded index polymer optical-fiber perform," *Opt. Laser Technol.*, vol. 40, pp. 687–691, 2008.

[21] Z. Zheng, H. Liang, H. Ming, Q. Zhang, Y. Yu, S. Liu, Y. Zhang, and J. Xie, "Rhodamine 6 G-doped polymer optical fiber amplifiers," *Chinese Opt. Lett.*, vol. 2, pp. 67–68, 2004.

[22] D. P. Gang, P. K. Chu, Z. Xiong, T. W. Whitbread, and R. P. Chaplin, "Dye-doped step-index polymer optical fiber for broadband optical amplification," *J. Lightw. Technol.* vol. 14, no. 10, pp. 2215–2223, Oct. 1996.

Authors' biographies not included at authors request due to space constraints.